Electrocatalysis
https://doi.org/10.1007/s12678-024-00886-7

RESEARCH

In Situ Synthesized Gold-Conjugated Hemoglobin-$Cu_3(PO_4)_2$ Hybrid Nanopetals for Enhanced Electrochemical Detection of H_2O_2

Mallesh Santhosh[1] · **Tusan Park**[1,2]

Accepted: 6 August 2024

Abstract

In situ synthesis of novel hybrid organic–inorganic nanopetals (HNPs) of Copper (Cu^{2+}) and gold-conjugated hemoglobin (Au@Hb) is reported. The presence of Au within the protein matrix prevents the formation of a flower-like assembly of the formed nanopetals of Au@Hb and Cu^{2+} via the co-precipitation method. Morphological, chemical, and electrocatalytic activities of in situ synthesized Au@Hb-Cu HNPs were examined systematically. The hybrid nanopetal (Au@Hb-Cu HNP)-modified screen-printed PET electrodes show enhanced electrocatalytic activity toward the oxidation of H_2O_2 compared to electrodes modified with Hb-copper hybrid nanoflowers (Hb-Cu HNFs) without Au conjugation. The proposed biosensor exhibits excellent electrochemical performance with broad linear responses over a H_2O_2 concentration ranging from 5 to 1000 µM ($R^2 = 0.99$) and showed a lower detection limit of 1.46 µM at 0.30 V vs. pseudo Ag/AgCl. Enhanced electrochemical performance is attributed to heterogeneous active sites over hybrid nanopetal surfaces. Moreover, the hybrid nanopetal–modified electrodes showed excellent stability and anti-interference performance in the presence of ascorbic acid, uric acid, fructose, and glucose. These results demonstrate that Au@Hb-Cu HNPs offer a better and more promising alternative for the electrochemical detection of H_2O_2 sensitively.

Keywords Biosensor · Hydrogen peroxide · Nanopetals · Hemoglobin · Hybrid nanostructure

Introduction

Hydrogen peroxide (H_2O_2) is a common chemical used in many industries such as food, biomedical, and pharmaceutical and is generally found in various biological environments as an important intermediate or final product of various enzymatic reactions which involve enzymes such as glucose oxidase (GOx) and alcohol oxidases [1, 2]. H_2O_2 also plays a crucial role in cellular mechanisms, is required in the production of various reactive oxygen species (ROS), serves as cellular signaling molecules, and governs various physiological processes such as cell differentiation, proliferation, and cellular metabolism [3]. Higher concentrations of H_2O_2 involve oxidative stress; can damage DNA, cellular proteins, and lipids; and cause diseases such as cancers, myocardial infarction, Alzheimer's, and atherosclerosis [4, 5]. In food and beverages, H_2O_2 residues can be found in the final products after pasteurization, sterilization, and packaging. H_2O_2 concentration above a certain threshold is considered hazardous for consumption [6]. For these diverse roles of H_2O_2 in industrial and biological processes, monitoring H_2O_2 has been an attractive target for researchers for many years. Currently, there are numerous analytical techniques available to detect H_2O_2 which include titrimetry [7], chromatography [8], chemiluminescence [9, 10], fluorometric [11, 12], spectrophotometric [13, 14], and electrochemical methods [1, 15–17].

For developing a H_2O_2 sensor, usually, strong redox activity of H_2O_2 was exploited through colorimetric method (via formation or degradation of dye) or electrochemical method (oxidizing a mediator) [6]. Among different transducing principles employed for H_2O_2, electrochemical methods have the advantages of simple instrumentation, low cost, high sensitivity, and fast response [18]. Numerous electrochemical H_2O_2 sensors, including enzyme and non-enzyme-based sensors, have previously been reported. In particular, electrochemical biosensors based on enzymes and other

✉ Tusan Park
tusan.park@knu.ac.kr

[1] Smart Agriculture Innovation Center, Kyungpook National University, Daegu, Republic of Korea

[2] Department of Smart Bio-Industrial Mechanical Engineering, Kyungpook National University, Daegu, Republic of Korea

Published online: 17 August 2024

proteins such as horse radish peroxidase (HRP) [7, 19, 20], catalases [21, 22], cytochrome C, and hemoglobin (Hb) [23–25] are the main focus in developing selective detection platform for H_2O_2 sensing. Among these heme proteins, Hb is mostly preferred because of its structural stability, commercial availability, and low cost, even though it displays weak catalytic activity compared to HRP, which is due to the deeply buried iron-containing heme active site [26]. A common strategy mostly utilized to enhance catalytic activity and improve stability is the immobilization of Hb on various nanomaterials which favorably exposes active sites and enhances activity. Notably, Hb immobilization on porous iron oxide, palladium, and multi-walled carbon nanotube (MWCNT) composite electrode [27], CNT-mesoporous silica hybrid electrode, Hb-DNA conjugate on nano-porous gold electrode [28], and graphene nanocomposite with different morphologies has been explored by the previous researcher. Conventional immobilization strategies such as adsorption, covalent, crosslinking, and entrapment ensure stability but often fail to maintain biological activity for longer periods. Recently, a novel immobilization approach was reported by Ge and co-workers when they discovered that the flower-like organic–inorganic hybrid nanostructure composed of enzyme and Cu^{2+} ion exhibited much higher enzyme activity and stability than free and conventional immobilized enzymes [29]. This has encouraged researchers to explore various enzymes, metal ions, and combinations of different enzymes to design new and innovative hybrid nanoflowers (HNFs) tailored for applications such as sensing, catalysis, biomedicine, and adsorption [30–34]. Previously, dual colorimetric/fluorescence biosensors were developed utilizing Hb and copper phosphate HNFs to detect H_2O_2 [31]. The same group utilized Hb-$Mn_3(PO_4)_2$ HNFs as a biocatalyst applied in an electrochemical platform to detect H_2O_2 on a glassy carbon electrode surface [35]. These studies prove that the hybrid structure facilitates adequate exposure of heme active sites of Hb and improves bio-catalytic and electrochemical performance. Apart from these, the electrochemical performances of these nanostructures are rarely explored, although these hybrid materials possess reasonably good design in terms of stability and catalytic activity. To efficiently utilize these nanostructures for electrochemical-based assay, HNFs of glucose oxidase (GOx) and HRP were utilized in combination with gold nanoparticle (AuNP)-decorated graphene fibers [36] for highly sensitive glucose sensing. A highly robust redox probe was also developed for electrochemical immunoassay by utilizing AuNP-conjugated HNFs of BSA and copper [37]. These methods exploit the unique properties of HNFs post-modified with nanomaterials to create high-performance probes for electrochemical sensing. Recently, in situ modification HNFs with nanomaterials such as magnetic nanoparticles [37] and carbon nanotubes (CNTs) [26] were demonstrated as a highly effective design strategy to create conjugates of HNFs with nanomaterials for highly sensitive glucose and peroxide sensing, respectively. The electrochemical method offers an affordable and easy-to-use solution yet provides a sensitive response with a fast response time. An effective immobilization strategy such mineralization of enzymes or proteins into flower-like structures not only enhances the stability of the enzymes but also increases catalytic activity. Furthermore, conjugation with nanomaterials such as AuNPs and graphene enables the utilization of hybrid nanoflower for enhanced electrochemical detection. However, the process of conjugation with nanomaterials usually involves additional steps [36, 37].

In this work, we report the in situ synthesis of Au-conjugated Hb-$Cu_3(PO_4)_2$ organic–inorganic hybrid nanopetals (Au@Hb-Cu HNPs) through a facile synthesis strategy for the first time. These hybrid nanopetals were utilized for sensitive electrochemical detection of H_2O_2 by depositing over a screen-printed carbon electrode (SPCE) on a flexible polyethylene terephthalate (PET) substrate. We revealed that the Au@Hb-Cu HNP-modified electrodes observed enhanced electrocatalytic activity toward the oxidation of H_2O_2 compared to electrodes modified with Hb-copper hybrid nanoflowers (Hb-Cu HNFs) without Au conjugation. The electrochemical biosensor based on Au@Hb-Cu HNPs exhibits high selectivity and good stability for determining H_2O_2.

Materials and Methods

Chemicals and Reagents

Hemoglobin (Hb) from human blood, H_2O_2 (30%, w/v), ascorbic acid (AA), glucose, uric acid (UA), fructose, copper sulfate pentahydrate, phosphate buffer saline (PBS) tablet, gold (III) chloride trihydrate ($HAuCl_4$), and Ag/AgCl conductive ink were purchased from Sigma-Aldrich (St. Louis, MO, USA). Polyethylene terephthalate (PET) transparent film was purchased from a local store. Carbon ink was purchased from Asahi CRL (Gifu, Japan). All other reagents were of analytical grade and used without further purification. All solutions were prepared using deionized water (18.2 MΩ).

Instrumentation

Screen printing on PET sheets was conducted on a custom-made screen-printing apparatus with a silk screen frame with a mesh size of 100. The three-electrode system with carbon ink as working and counter electrode and Ag/AgCl ink as pseudo reference ink was screen printed on the PET substrate. All electrochemical work including cyclic voltammetry (CV), amperometry, and electrochemical impedance spectroscopy (EIS) experiments was carried out using

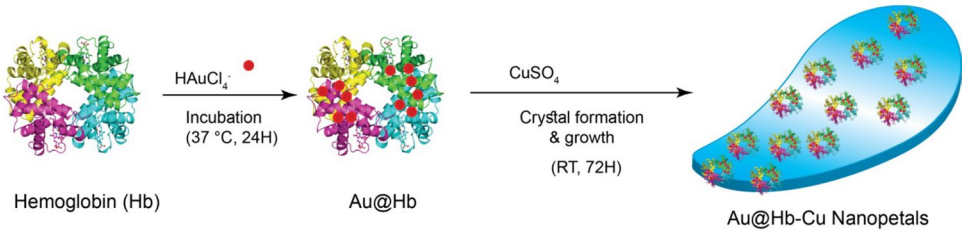

Scheme 1 Schematic representation of Au@Hb-Cu nanopetal formation

PalmSens4 (Netherland) electrochemical interface. The surface morphologies of the synthesized hybrid nanopetals were characterized by the field emission scanning electron microscope (FESEM) equipped with energy dispersive X-ray (EDX) analyzers (SU8220, Hitachi). Ultraviolet–visible (UV–vis) absorption spectra were obtained using a USB4000-UV–VIS spectrometer (Ocean Optics, USA). X-ray photoelectron spectra (XPS) of hybrid nanopetals were characterized by an X-ray photoelectron spectrometer (NEXSA, Thermo Fisher).

Synthesis of Au@Hb-Cu HNPs

In a typical experiment, an aqueous solution of $HAuCl_4$ (5 mM, 5 ml) was added to 5 ml of Hb (1 mg ml^{-1}) in PBS (0.1 M. pH 7.4). Both solutions were mixed together for 10 min and kept for incubation overnight at 37 ℃. $CuSO_4$ (120 mM, 60 µl) was added to the above solution and incubated for 72 h at room temperature (RT). After incubation, the precipitates were collected by centrifugation (3500 rpm for 5 min), and the precipitate was washed several times with ultra-pure water and stored at 4 °C. The representation of the synthesis of Au@Hb-Cu HNPs was shown in Scheme 1. Furthermore, for comparison studies, Hb-$Cu_3(PO_4)_2$ HNFs were also prepared under similar concentration and experimental conditions.

Preparation of Au@Hb-Cu HNP-Modified SPCE

The preparation of the modified electrode was carried out by drop casting 3 µl of Au@Hb-Cu HNP solution (1 mg ml^{-1}) on the working electrode area and later allowed to dry at RT. The modified electrodes were stored at 4 °C. Similarly, Hb-Cu HNF-modified electrodes were also prepared for the comparison analysis.

Measurement of Electrochemical Properties

Electrochemical measurements for the characterization of the prepared sensor were carried out by using CV, EIS, and chronoamperometric (CA) methods. UA, AA, fructose, and glucose were selected as coexisting substances to evaluate the anti-interference ability of the prepared hybrid electrodes.

Results and Discussion

Chemical Characterization of Au@Hb-Cu HNPs

The synthesized nanostructures were characterized by using UV–vis and XPS techniques. Figure 1A represents the UV–visible spectra of Hb, Hb-Cu HNFs, and Au@Hb-Cu HNPs and inorganic copper phosphate ($Cu_3(PO_4)_2$) nanocrystals (NCs). The typical Soret band corresponding to pure Hb (red trace) was observed around 405 nm, which is due to the specific absorption of the heme prosthetic group [38]. $Cu_3(PO_4)_2$ NCs (blue trace) do not have any features around this region, whereas Hb-Cu HNF spectra (green trace) show a broader Soret absorption peak around 410 nm, with a 5 nm shift from pure Hb sorbet peak. This is accounted for by the interaction between the Hb and copper phosphate. The absorption spectra for Au@Hb-Cu nanostructure and the signal intensity of the Soret band decreased and broadened, and its peak position was also revealed to be slightly blue-shifted from 405 nm, as shown in the UV–vis absorption spectrum as represented in Fig. 1A (black trace). The decrease in the signal intensity and blue-shift of the peak position observed can be attributed to changes in the hydrophobicity of heme groups due to the formation of Au conjugation on the Hb molecule [39]. Moreover, the reaction at physiological temperature produces small gold clusters after 24 h incubation, whereas the formation of bigger nanoparticles of different shapes and sizes was reported to be produced at higher temperatures [40].

The chemical compositions of Au@Hb-Cu HNPs were analyzed by XPS. Figure 1B represents the survey spectrum of the synthesized Au@Hb-Cu HNPs. The spectrum clearly reveals that the synthesized Au@Hb-Cu HNPs are mainly composed of C, N, O, Cu, and Au. Figure 1C depicts the C 1 s spectrum where de-convoluted peaks at 284.69 eV, 285.61 eV, and 287.73 eV are attributed to aliphatic, aromatic, and carbonyl carbon atoms of Hb protein moiety, respectively. The N 1 s spectrum (Fig. 1D) has a peak at 399.53 eV which corresponds to amide in the Hb protein in the hybrid nanostructure. The spectrum of O 1 s shows a peak at 531.28 eV and corresponds to OH and C = O groups (Fig. 1E). The XPS spectrum of Au 4f (Fig. 1F) shows binding energy peaks of 88.3 eV and 84.6 eV and corresponds to Au $4f_{5/2}$ and Au $4f_{7/2}$, respectively, which are attributed

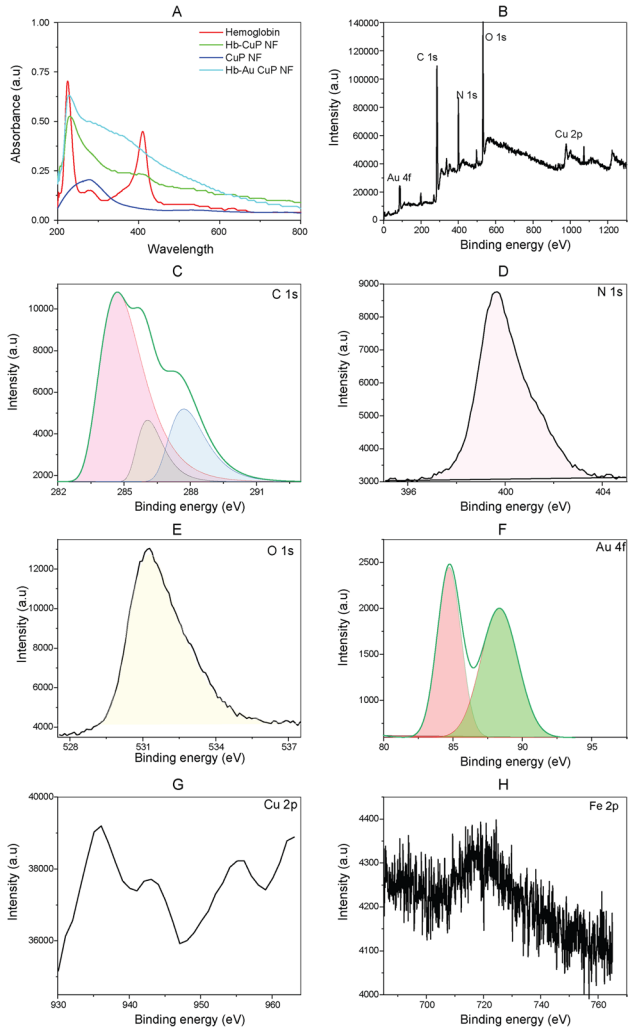

Fig. 1 (**A**) UV-vis spectra of Hb (red trace), $Cu_3(PO_4)_2$ nanocrystals (pink trace), Hb-Cu HNFs (green trace), and Au@Hb-Cu HNPs (black trace). XPS spectra of Au@Hb-Cu HNPs (**B**) survey spectrum, C 1 s (**C**), N 1 s (**D**), O 1 s (**E**), Au 4f (**F**), Cu 2p (**G**), and Fe 2P (**H**)

to spin–orbit coupling state of Au. XPS spectrum for Cu 2P which belongs to the inorganic part ($Cu_3(PO_4)_2$) is represented in Fig. 1G. The peak corresponds to Cu $2p_{1/2}$ and Cu $2p_{3/2}$ and was observed at 955.08 eV and 936.08 eV, respectively, representing the adequately exposed Cu active sites on the surface of the hybrid nanopetals [41]. The binding energy peak of Fe 2p (710 eV) in the XPS spectra (Fig. 1H) also indicates that Fe exists in Au@Hb-Cu HNP hybrid nanostructures.

Morphological Characterization of Au@Hb-Cu HNPs

The formation mechanism of hybrid organic–inorganic nanoflowers (HNFs) was studied previously [42]. Accordingly, the mechanism of HNF growth begins with the formation of nucleation sites and subsequent growth to form nanopetals and the arrangement of nanopetals into 3D hierarchical nanoflower-like structures. Firstly, crystals of copper phosphate formed when Cu^{2+} ions interact with phosphate ions of PBS solution. Then, the amide backbone of the protein forms coordination with copper phosphate crystal to form a protein-Cu complex. These complexes act as nucleation sites, grow with reaction time, form nanopetals, and are arranged subsequently to form hybrid nanoflowers [29]. Figure 2 represents FESEM images of $Cu_3(PO_4)_2$ nanocrystals (A), Hb-Cu HNFs (B), and Au@Hb-Cu HNPs (C and D). In the absence of protein, irregular-sized, non-uniform morphology nanocrystals of $Cu_3(PO_4)_2$ formed as shown in Fig. 2A. In the presence of Hb, a 3D hierarchical hybrid nanoflower-like structure appeared with uniform architecture as shown in Fig. 2B. The average diameter of these Hb-Cu HNFs was found to be ~ 6 μm (Supplementary Fig. S1), which is consistent with the previously reported Hb-Cu HNFs [31]. Figure 2C, D represents the FESEM images of the Au@Hb-Cu nanostructure. Uniform, nano-seized, flower petal–like structures were observed. Notably, flower-like morphology was not observed when Au@Hb was utilized instead of Hb for the construction of a hybrid organic–inorganic nanostructure. Instead, uniform-sized nanopetals with uniformly decorated AuNPs were observed, indicating that the Au prevented the nanopetals from being arranged into nanoflower-like structures. Previously, it was also reported that the presence of Au NPs did not aid the formation of nanoflowers [43].

The elemental X-ray mapping of control and Au@Hb-Cu HNPs was also carried out using EDX analysis. Figure 2E, F represents the SEM images and corresponding X-ray mapping analysis images of Hb-Cu HNFs and Au@Hb-Cu HNPs, respectively. These clearly show the presence of Au, Cu, and Fe confirming the gold nanoparticle–decorated Hb-Cu hybrid nanopetal structure as compared to Hb-Cu HNFs. The presence of Au in these hybrid nanopetal structures was also confirmed in the previous section by XPS studies.

Electrochemical Characterization of the Au@Hb-Cu HNP-Modified Screen-Printed Carbon Electrode (SPCE)

Electrochemical features of the Au@Hb-Cu HNP- and Hb-Cu HNF-modified SPCEs were studied by EIS and CV techniques. Figure 3A represents EIS spectra as Nyquist plots of the modified electrodes in a PBS solution containing 5.0 mM $[Fe(CN)_6]^{3-/4-}$ and 0.1 M KCl. The plots were fitted with the equivalent circuit shown in the inset of Fig. 3A [44]. The high-frequency intercept at the Z_{re} axis corresponded to the ohmic resistance (R_e), which represented the resistance of the electrolyte, and the semicircle in the middle-frequency range indicated the resistance to charge transfer (R_{ct}). These values vary and are strongly dependent on different modifications of the electrode surface. The extrapolated data from the Randell

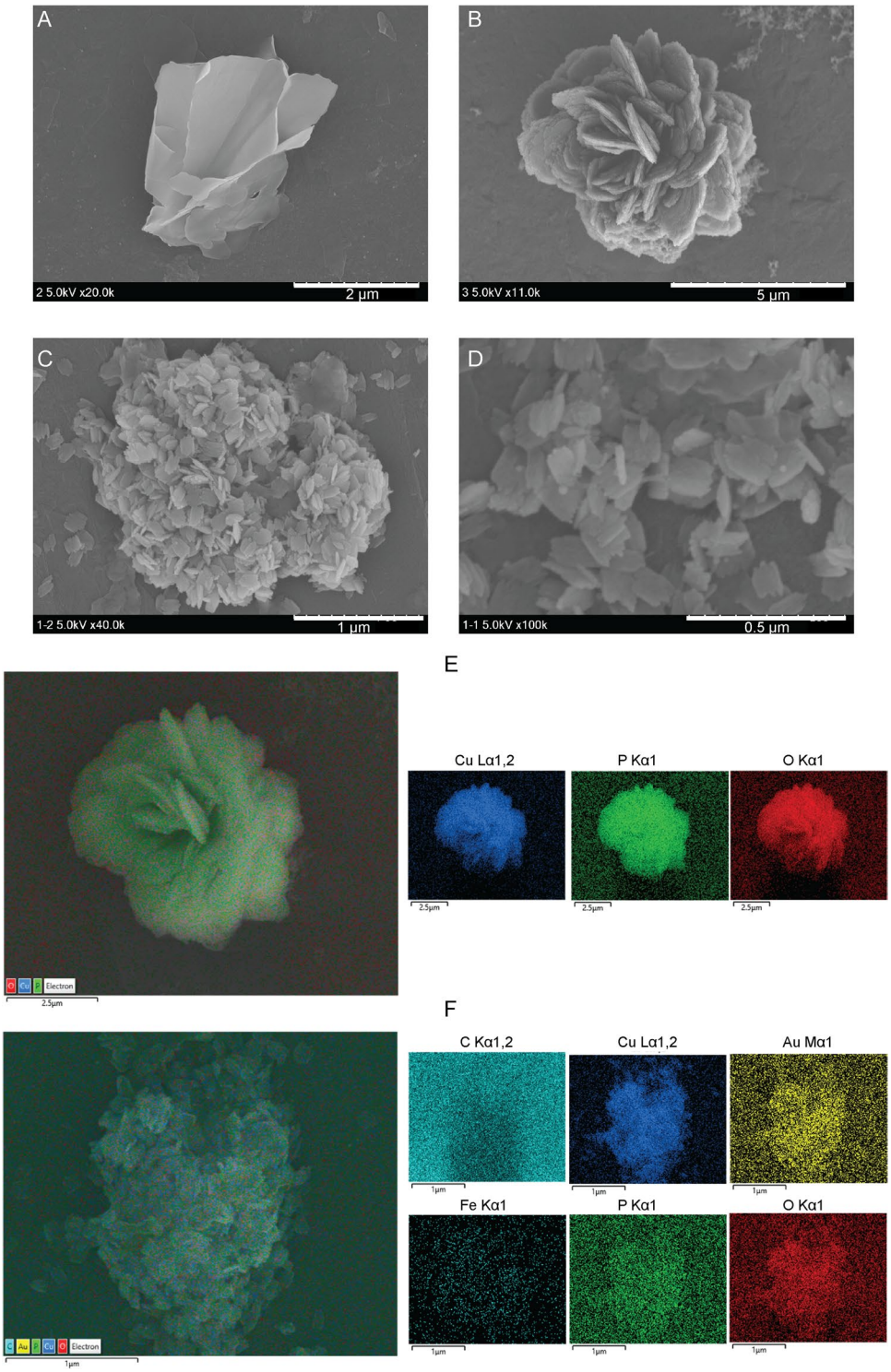

Fig. 2 FESEM images of **A** $Cu_3(PO_4)_2$ nanocrystals, **B** Hb-Cu HNFs, **C** Au@Hb-Cu HNPs, and **D** magnified view of Au@Hb-Cu HNPs. Elememtal X-ray mapping of **E** Hb-Cu HNFs and **F** Au@Hb-Cu HNPs

circuit is fitted with EIS data from individual electrodes and tabulated in table S1. From the fitted parameters, the charge transfer resistance of Hb-Cu HNFs was relatively higher than that of bare electrodes, which is attributed to the fact that most of the biological molecules are poor electrical conductors and cause hindrance to electron transfer [45], whereas, after the modification of the electrode with Au@Hb-Cu HNPs, the R_{ct} decrease significantly, and a semicircle of the Nyquist plot was approximately a straight line compared to the bare electrode (Fig. 3A red trace). These studies suggest that the in situ formed Au@Hb conjugate of the hybrid nanopetals facilitated the electron transfer. Previous reports of enhanced electron transfer kinetics of Hb-Au nanocomposite [46] and hybrid

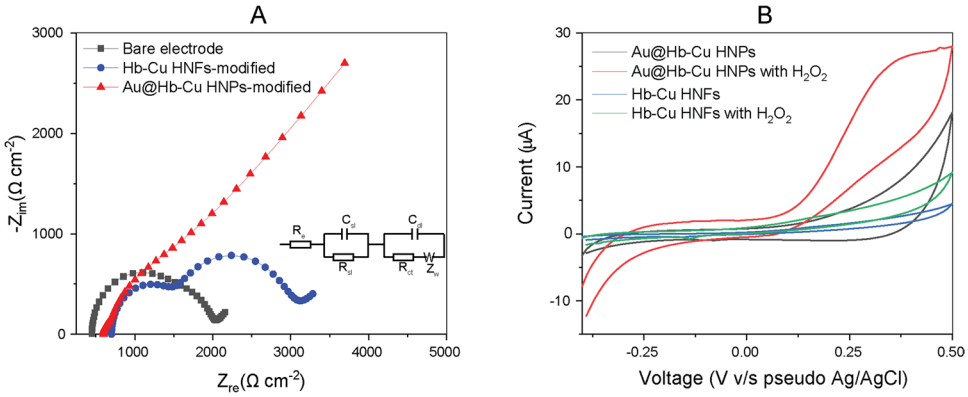

Fig. 3 **A**, **B** EIS spectra represented as Nyquist plot of bare (black trace) and Hb-Cu HNF-modified (blue trace) and Au@Hb-Cu HNP-modified (red trace) SPCEs. Inset: equivalent circuit diagram. CV curves of Hb-Cu HNF- and Au@Hb-Cu HNP-modified electrode in the absence (blue and black trace) and presence of H_2O_2 (green and red trace), respectively

nanoflower–conjugated AuNPs [34] suggest the favorable role of Au nanostructure for facile electron transfer.

The CV studies were carried out to investigate the catalytic activity of the Au@Hb-Cu HNP- and Hb-Cu HNF-modified electrodes. Figure 3B represents the cyclic voltammogram of the Hb-Cu HNF- and Au@Hb-Cu HNP-modified electrode in the absence (blue and black trace) and presence of H_2O_2 (green and red trace), respectively. The background current on Au@Hb-Cu HNPs is higher than that of Hb-Cu HNF-modified electrodes, indicating improved electrocatalytic surface area. Both electrodes respond with the increased anodic and cathodic current when H_2O_2 is introduced. Hb-Cu HNF-modified electrodes provide a weak response, while Au@Hb-Cu HNP-modified electrodes display a more current response demonstrating that the hybrid nanopetal–modified electrode possesses good electrocatalytic activity toward the oxidation of H_2O_2. In the case of Au@Hb-Cu HNP-modified electrode, the presence of nano-sized, uniform petals decorated from Au prevented larger flower formation and provided a larger electroactive surface with more electroactive center for enhanced electrocatalytic activity toward H_2O_2. Besides this, both Cu and Au have excellent electronic conductivity, while Cu is known to possess excellent electrocatalytic activity. According to previous studies, the coordination between the Cu atom and the carboxyl O atom from amino acid results in the formation of the Cu–O bond on nanopetal formation. In this hybrid structure, CuO was deemed as the dominant sensing part catalyzing H_2O_2 oxidation [47]. The reaction mechanism of hybrid nanopetal structure towards oxidation of H_2O_2 is demonstrated through the following equation:

$$2CuO + H_2O_2 \rightarrow Cu_2O + H_2O + O_2$$

The improvement of electrochemical performance of Au@Hb-Cu HNP-modified electrode toward electro-catalysis of H_2O_2 may be attributed to the unique heterostructure with the presence of exposed electroactive sites made from the clusters of Au and Cu over nano-sized petals of Au@Hb-Cu hybrid structure. It is reported that nano-micro-sized gold structure–decorated CuO framework was demonstrated to be the effective design for the electro-catalysis of H_2O_2, where the presence of Au enhances the higher adsorption of H_2O_2 and enhanced charge distribution toward H_2O_2 catalysis [48]. This might be the reason that the electrode modified with Au@Hb-Cu HNPs expressed an increase in both oxidation and reduction current in the presence of H_2O_2 compared to Hb-Cu HNF-modified electrodes.

Figure 4A illustrates the CVs recorded using Au@Hb-Cu HNPs with different scan rates from 10 to 100 mV s^{-1} in 0.1 M PBS. When the scan rate increases, the redox peak currents corresponding to the Au@Hb-Cu HNPs are increased. At the same time, the peak potential was shifted a bit toward the higher positive potential. The linear plot was made between the scan rate and the redox peak currents of Au@Hb-Cu HNPs which showed the linear regression equation with the R^2 values of 0.98 and 0.99 for the oxidation and the reduction peak currents, respectively (Fig. 4B), which is anticipated for successful immobilization and surface-confined Au@Hb-Cu HNP-modified electrode (Fig. 5).

Au@Hb-Cu HNP-Modified SPCE for H_2O_2 Sensing

The CV curves of a Au@Hb-Cu HNP-modified SPCE in the presence of H_2O_2 display the increases in anodic current beyond 0.3 V vs. pseudo Ag/AgCl (as shown in Fig. 3D). Chronoamperometry (CA), which measures current in the sensor over time with the analyte, is conducted to generate current–time (I–T) curve. Figure 4A shows the CA curves recorded at the Au@Hb-Cu HNP-modified SPCE at various concentrations of H_2O_2 at an applied potential of 0.3 V vs. pseudo Ag/AgCl. The steady-state current for each H_2O_2 concentration is plotted against H_2O_2 concentration to extract a linear fit and thus a sensitivity, as shown in Fig. 4B, where the current recorded at 10 s is plotted against the corresponding H_2O_2 concentration. To compare the advantage of Au@Hb-Cu HNP- over Hb-Cu HNF-modified SPCE, CA measurements were also carried out for

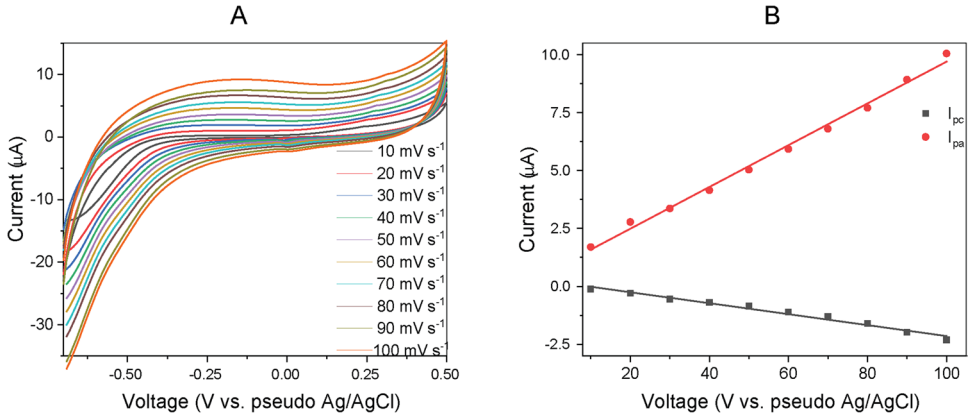

Fig. 4 **A** Cyclic voltammogram responses of Au@Hb-Cu HNP-modified SPCE at different scan rates. **B** The fitted curve of peak current density responses versus scan rate

Hb-Cu HNF-modified SPCE at different H_2O_2 concentrations at 0.3 V vs. pseudo Ag/AgCl. At an applied potential of 0.3 V, the Au@Hb-Cu HNP-modified electrode exhibited a long linear response range from 5 μM to 1.0 mM and an excellent sensitivity of 22.53 ± 0.6 μA mM^{-1} cm^{-2} and a low theoretical detection limit of 1.46 ± 0.8 μM which is calculated from the $3 \times$ SD of blank/slope of the response curve generated at lower H_2O_2 concentration (supplementary Fig. S2). Compared with the Hb-Cu HNF-modified SPCE (supplementary Fig. S3A and B), the Au@Hb-Cu HNP-modified electrode exhibited superior performance (Fig. 3C and D) largely due to the sufficient synergetic effect between heterogeneous active sites and larger specific area of these hybrid Au@Hb-Cu HNPs, which contributes to the excellent electrocatalytic activity toward H_2O_2.

The sensing performance of the prepared Au@Hb-Cu HNP-modified SPCE is also compared with recently reported enzymatic and non-enzymatic electrochemical sensors and tabulated in Table 1. Compared with the reports, our biosensor possesses a wider linear range compared with enzymatic sensors and exhibits extremely good sensitivity comparable with both enzymatic and non-enzymatic sensors, indicating the superior electrocatalytic ability of this heterostructure with the abundant active site available for the electro-catalysis and electron transfer on the nanopetal surface. Moreover, our sensors fabricated on a disposable flexible PET platform offer a simple and inexpensive way for rapid on-site analysis. Thus, the Au@Hb-Cu HNP-modified electrode holds the promising potential to be applicable in real sample applications, where high sensitivity is required.

Selectivity, Repeatability, and Stability Analysis of the Biosensor

The selectivity of the developed Au@Hb-Cu HNP electrochemical biosensor was examined by monitoring the effect of possible interfering substances on H_2O_2 determination. For this purpose, the CA measurements were performed for H_2O_2 (1.0 mM) and potentially interfering compounds such as ascorbic acid, glucose, fructose, and uric acid in the same concentration (1.0 mM) at optimized working conditions. With the addition of the interferent molecules, a negligible change in the current signal intensity was observed, but with the introduction of H_2O_2, a significant increase in the current response (Fig. 6A) indicates that the developed disposable biosensor based on Au@Hb-Cu HNPs can be utilized for interference-free detection of H_2O_2.

The current response on three different Au@Hb-Cu HNP-modified SPCEs at 1.0 mM H_2O_2 concentration was represented in Fig. 6B. Relative standard deviation (RSD) value of 4.20 was obtained between the electrodes indicating that the Au@Hb-Cu HNP-modified SPCE is highly reproducible. The current response Au@Hb-Cu HNP-modified

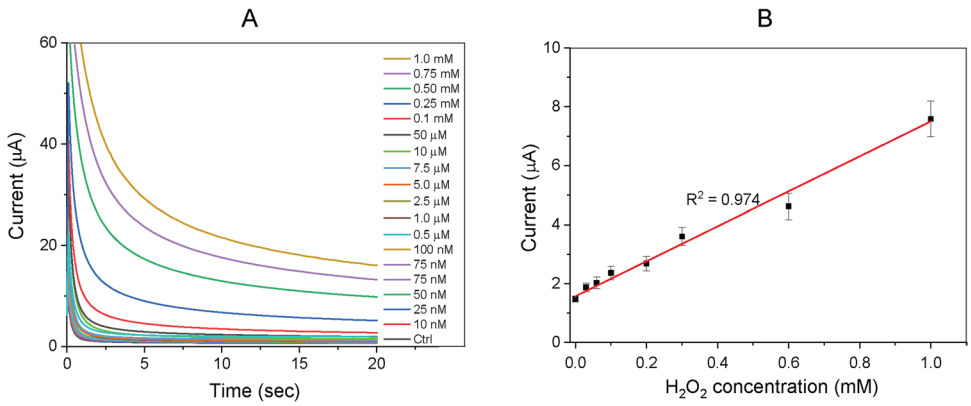

Fig. 5 **A** Amperometric responses of the Au@Hb-Cu HNP-modified SPCE with different concentrations of H_2O_2. **B** Calibration curve generated from the response of modified electrode on H_2O_2 concentration

Table 1 Comparison of sensing performance of recently published H_2O_2 sensors

Electrode modifification	Applied potential (V)	Limit of detection (LOD)	Sensitivity (μA mM^{-1} cm^{-2})[a]	Detection range	Reference
Iridium complex MS/CPE	0.6	2.6 μM	NA	51.5 to 508.2 μM	[49]
Vertically aligned Au-NW	-0.3	12 μM	250	40 μM to 15 mM	[15]
Hb-Mn HNFs	-0.15	0.007 μM	68.94	20 nM to 3.6 μM	[35]
CuO/BP	0.3	0.03 μM	1.70	40 to 480 μM	[41]
			0.58	480 μM to 9.20 mM	
AGCE	-0.4	53 μM	0.17	0.1 to 10 mM	[50]
AuNFs/Fe_3O_4@ZIF-8-MoS_2/GCE	-0.55	0.9 μM	41.7	5 to 120 mM	[51]
AuNFs/(PEI/PAA)/GR/GCE	-0.4	4.5 μM	50.07	5 to 5000 μM	[52]
Au@Hb-Cu HNPs/SPCE	0.30	1.46 μM	22.53	5 to 1000 μM	Current work

MS microsphere, CPE carbon paste electrode, Au-NW gold nanowire, Hb-Mn HNFs hemoglobin-manganese hybrid nanoflowers, CuO copper oxide, BP black phosphorous, AGCE activated glassy carbon electrode, AuNFs gold nanoflowers, Fe3O4 iron oxide, MoS2 molybdenum disulfide, GR graphene.[a]Normalized results.

SPCE was repetitively measured five times for 1.0 mM H_2O_2 concentration and found an RSD value of 3.64 between the measurements which proves the repeatability of the biosensor (Fig. 6C). The long-term stability of Au@Hb-Cu HNP electrodes was examined by measuring current response to 1.0 mM of H_2O_2 for 5 consecutive weeks. The modified electrodes maintained almost the same response at the end of the 5th week compared to the 1st week (Fig. 6D). All these results suggest that the Au@Hb-Cu HNP-modified biosensor demonstrated excellent performance for H_2O_2 detection.

The amperometric measurement of the H_2O_2-spiked tap water sample was performed to examine the potential of the developed sensor to analyze real samples. The tap water samples were spiked with a known concentration of H_2O_2, and the amperometric current response of Au@Hb-Cu HNP-modified SPCE was monitored at 0.30 V (vs. pseudo Ag/AgCl). The results were tabulated in supplementary table S2. The present method exhibited good recovery of 97–98%, with the least RSD values, suggesting that the developed bio-electrode can be implemented for measuring H_2O_2 in real samples.

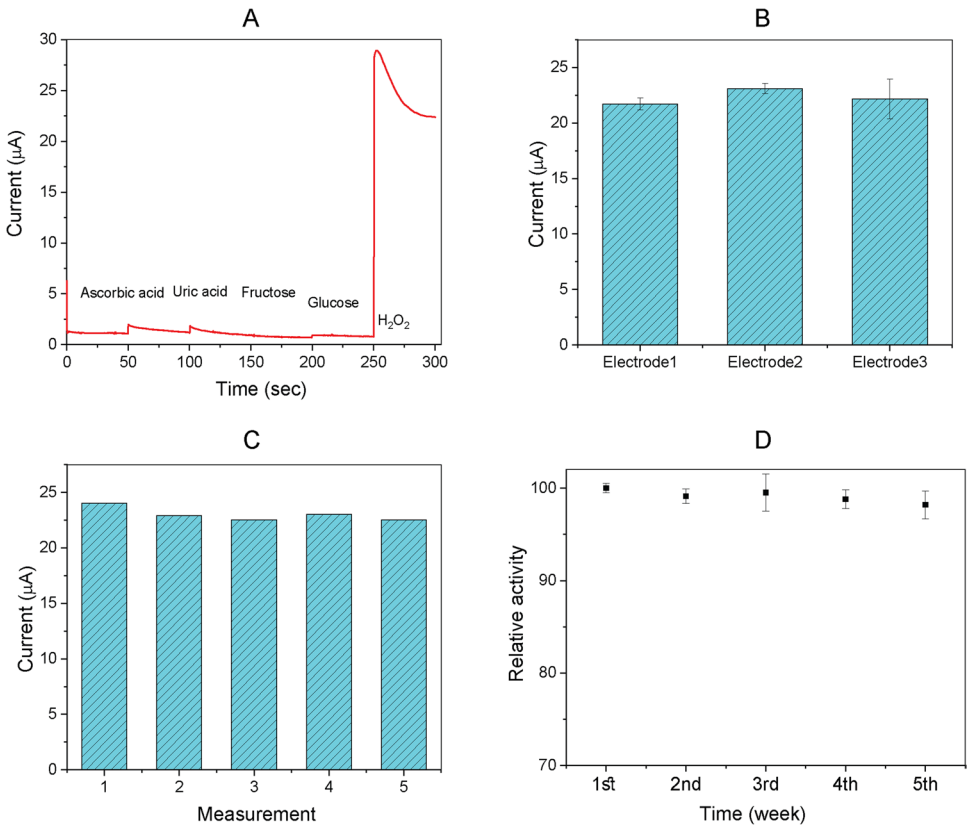

Fig. 6 **A** Effect of interfering species ascorbic acid, uric acid, fructose, and glucose on the amperometric response of Au@Hb-Cu HNP-modified electrode for H_2O_2 detection. **B** Reproducibility of three different Au@Hb-Cu HNP-modified electrodes for the detection of H_2O_2 and **C** repeatability of Au@Hb-Cu HNP-modified electrode for five successive measurements of H_2O_2. **D** Stability studies of Au@Hb-Cu HNPs for 5 weeks

Conclusion

In summary, we have successfully fabricated an electrochemical biosensor based on Au@Hb-Cu hybrid nanopetals for sensitive detection of H_2O_2. The hybrid nanopetal–based sensors demonstrated good catalytic activity toward H_2O_2 due to the presence of a highly dense active site over the hybrid nanopetal surface and the availability of a larger surface area. Uniform-sized nanopetals of Au@Hb conjugates prevent the assembly of these nanopetals into dense flower-like structures. Moreover, the presence of heterogeneous active sites of Au and Cu has a synergetic effect on the electro-catalysis of H_2O_2. Consequently, the Au@Hb-Cu HNP-modified electrode has better performance than the Hb-Cu HNF-modified electrode. The constructed biosensor possesses a good low limit of detection and has a wide linear detection range. Additionally, the biosensor shows interference-free detection of H_2O_2 and has favorable reproducibility with good stability.

Supplementary Information The online version contains supplementary material available at https://doi.org/10.1007/s12678-024-00886-7.

Acknowledgements This work was supported by the National Research Foundation of Korea(NRF) grant funded by the Korean government (Ministry of Science and ICT) (RS-2024-00338052). We also acknowledge the Center for Scientific Instruments, Kyungpook National University, Daegu for providing FESEM and XPS instrumentation for the analysis.

Declarations

Conflict of Interest The authors declare no competing interests.

References

1. S. Chen, R. Yuan, Y. Chai, F. Hu, Electrochemical sensing of hydrogen peroxide using metal nanoparticles: a review. Microchim. Acta **180**, 15–32 (2013). https://doi.org/10.1007/s00604-012-0904-4
2. G. Georgiou, L. Masip, An overoxidation journey with a return ticket. Science **300**(5619), 592–594 (2003)
3. T. Konno, E.P. Melo, J.E. Chambers, E. Avezov, Intracellular sources of ROS/H_2O_2 in health and neurodegeneration: spotlight on endoplasmic reticulum. Cells **10**(2), 233 (2021). https://doi.org/10.3390/cells10020233
4. B. Halliwell, M.V. Clement, J. Ramalingam, H.L. Lee, Hydrogen peroxide. Ubiquitous in cell culture and in vivo? IUBMB Life **50**, 251–257 (2000). https://doi.org/10.1080/15216540051080930
5. Y.A. Hajam, R. Rani, S.Y. Ganie, Oxidative stress in human pathology and aging: molecular mechanisms and perspectives. Cells **11**(3), 552 (2022). https://doi.org/10.3390/cells11030552
6. J.E. Giaretta, H. Duan, F. Oveissi, Flexible sensors for hydrogen peroxide detection: a critical review. ACS Appl. Mater. Interfaces **14**, 20491–20505 (2022). https://doi.org/10.1021/acsami.1c24727
7. Y.A. Woo, H.R. Lim, H.J. Kim, H. Chung, Determination of hydrogen peroxide concentration in antiseptic solutions using portable near-infrared system. J. Pharm. Biomed. Anal. **33**(5), 1049–1057 (2003). https://doi.org/10.1016/S0731-7085(03)00420-5
8. M. Song, J. Wang, B. Chen, L. Wang, A. Facile, Nonreactive hydrogen peroxide (H_2O_2) detection method enabled by ion chromatography with UV detector. Anal. Chem. **89**, 11537–11544 (2017). https://doi.org/10.1021/acs.analchem.7b02831
9. M.R. Jones, K. Lee, Determination of environmental H_2O_2 for extended periods by chemiluminescence with real-time inhibition of iron interferences. Microchem. J. **147**, 1021–1027 (2019). https://doi.org/10.1016/j.microc.2019.04.027
10. J. Mettakoonpitak, N. Sawatdichai, D. Thepnuan, A. Siripinyanond, Microfluidic paper - based analytical devices for simultaneous detection of oxidative potential and copper in aerosol samples. Microchim. Acta **190**, 241 (2023). https://doi.org/10.1007/s00604-023-05819-7
11. K. Sasakura, K. Hanaoka, N. Shibuya, Development of a highly selective fluorescence probe for hydrogen sulfide. J. Am. Chem. Soc. **133**, 18003–18005 (2011). https://doi.org/10.1021/ja207851s
12. E. Ortega, S. de Marcos, J. Galbán, Fluorometric enzymatic auto-indicating biosensor for H_2O_2 determination based on modified catalase. Biosens. Bioelectron. **41**, 150–156 (2013). https://doi.org/10.1016/j.bios.2012.08.001
13. K.B.R. Teodoro, F.L. Migliorini, W.A. Christinelli, D.S. Correa, Detection of hydrogen peroxide (H_2O_2) using a colorimetric sensor based on cellulose nanowhiskers and silver nanoparticles. Carbohydr. Polym. **212**, 235–241 (2019). https://doi.org/10.1016/j.carbpol.2019.02.053
14. J. Zou, H. Cai, D. Wang, Spectrophotometric determination of trace hydrogen peroxide via the oxidative coloration of DPD using a Fenton system. Chemosphere **224**, 646–652 (2019). https://doi.org/10.1016/j.chemosphere.2019.03.005
15. Q. Lyu, Q. Zhai, J. Dyson, Real-time and in-situ monitoring of H_2O_2 release from living cells by a stretchable electrochemical biosensor based on vertically aligned gold nanowires. Anal. Chem. **91**, 13521–13527 (2019). https://doi.org/10.1021/acs.analchem.9b02610
16. V. Patel, P. Kruse, P.R. Selvaganapathy, Solid state sensors for hydrogen peroxide detection. Biosensors **11**(1), 9 (2021). https://doi.org/10.3390/bios11010009
17. M. Baccarin, B.C. Janegitz, R. Berté, Direct electrochemistry of hemoglobin and biosensing for hydrogen peroxide using a film containing silver nanoparticles and poly(amidoamine) dendrimer. Mater. Sci. Eng. C **58**, 97–102 (2016). https://doi.org/10.1016/j.msec.2015.08.013
18. D.R. Thévenot, K. Toth, R.A. Durst, G.S. Wilson, Electrochemical biosensors: recommended definitions and classification. Anal. Lett. **34**, 635–659 (2001). https://doi.org/10.1081/AL-100103209
19. X.X. Xu, J.X. Zhang, F. Guo, A novel amperometric hydrogen peroxide biosensor based on immobilized Hb in Pluronic P123-nanographene platelets composite. Colloids Surf. B Biointerfaces **84**, 427–432 (2011). https://doi.org/10.1016/j.colsurfb.2011.01.037
20. J.H. Shin, M.J. Lee, J.H. Choi, Electrochemical H_2O_2 biosensor based on horseradish peroxidase encapsulated protein nanoparticles with reduced graphene oxide-modified gold electrode. Nano Converg. **7**, 39 (2020). https://doi.org/10.1186/s40580-020-00249-0
21. S. Dayan, N. Özdemir, N. Ibrahim, N. Kalayciog, Catalase / Fe_3O_4 @ Cu^{2+} hybrid biocatalytic nanoflowers fabrication and efficiency in the reduction of organic pollutants. Polyhedron **194**, 3–11 (2021). https://doi.org/10.1016/j.poly.2020.114888
22. L. He, W. Qian, L. Cen, Catalase-conjugated collagen surfaces and their application for the quantification determination of H_2O_2 in milk. Lwt **147**, 111601 (2021). https://doi.org/10.1016/j.lwt.2021.111601
23. A.K. Yagati, H.T. Le Ngoc, S. Cho, Bioelectrocatalysis of hemoglobin on electrodeposited ag nanoflowers toward H2O2 detection. Nanomaterials **10**, 1–13 (2020). https://doi.org/10.3390/nano10091628
24. Y. Yuan, X. Ni, Y. Cao, A magnetic electrode modified with hemoglobin for determination of hydrogen peroxide: distinctly

improved response by applying a magnetic field. Microchim. Acta **187**, 92 (2020). https://doi.org/10.1007/s00604-019-4061-x
25. R. Gao, Y. Song, Y. Gao, Stable hemoglobin-based biosensor based on coordination-assisted microfluidic technology for hydrogen peroxide determination. Sens. Actuators Rep. **5**, 100146 (2023). https://doi.org/10.1016/j.snr.2023.100146
26. S. Dadi, N. Temur, O.T. Gul, In situ synthesis of horseradish peroxidase Nanoflower@Carbon nanotube hybrid nanobiocatalysts with greatly enhanced catalytic activity. Langmuir **39**, 4819–4828 (2023). https://doi.org/10.1021/acs.langmuir.3c00260
27. M. Baghayeri, H. Veisi, Fabrication of a facile electrochemical biosensor for hydrogen peroxide using efficient catalysis of hemoglobin on the porous Pd@Fe_3O_4-MWCNT nanocomposite. Biosens. Bioelectron. **74**, 190–198 (2015). https://doi.org/10.1016/j.bios.2015.06.016
28. J. Jo, J. Yoon, T. Lee, H_2O_2 biosensor consisted of hemoglobin - DNA conjugate on nanoporous gold thin film electrode with electrochemical signal enhancement. Nano Converg. **6**, 1 (2019). https://doi.org/10.1186/s40580-018-0172-z
29. J. Ge, J. Lei, R.N. Zare, Protein – inorganic hybrid nanoflowers. Nat. Nanotechnol. **7**, 428–432 (2012). https://doi.org/10.1038/nnano.2012.80
30. M. Bilal, M. Asgher, S.Z.H. Shah, H.M.N. Iqbal, Engineering enzyme-coupled hybrid nanoflowers: the quest for optimum performance to meet biocatalytic challenges and opportunities. Int. J. Biol. Macromol. **135**, 677–690 (2019). https://doi.org/10.1016/j.ijbiomac.2019.05.206
31. J. Gao, H. Liu, L. Pang, Biocatalyst and colorimetric/fluorescent dual biosensors of H_2O_2 constructed via hemoglobin-Cu3(PO4)2 organic/inorganic hybrid nanoflowers. ACS Appl. Mater. Interfaces **10**, 30441–30450 (2018). https://doi.org/10.1021/acsami.8b10968
32. R. Jin, D. Kong, X. Zhao, Tandem catalysis driven by enzymes directed hybrid nanoflowers for on-site ultrasensitive detection of organophosphorus pesticide. Biosens. Bioelectron. **141**, 111473 (2019). https://doi.org/10.1016/j.bios.2019.111473
33. C. Tong, H. Liu, Y. Mo, In-situ growth of enzyme/copper phosphate hybrids on carbon cloth surface as self-powered electrochemical glucose biosensor. Biochem. Eng. J. **193**, 108860 (2023). https://doi.org/10.1016/j.bej.2023.108860
34. Z. Wang, J. Tu, P. Dong, BSA-$Cu_3(PO_4)_2$ hybrid nanoflowers as a high-performance redox indicator for robust label-free electrochemical immunoassay. Anal. Chim. Acta **1210**, 339873 (2022). https://doi.org/10.1016/j.aca.2022.339873
35. J. Gao, H. Liu, C. Tong, Hemoglobin-$Mn_3(PO_4)_2$ hybrid nanoflower with opulent electroactive centers for high-performance hydrogen peroxide electrochemical biosensor. Sens. Actuators B Chem. **307**, 127628 (2020). https://doi.org/10.1016/j.snb.2019.127628
36. S.H. Baek, J. Roh, C.Y. Park, Cu-nanoflower decorated gold nanoparticles-graphene oxide nanofiber as electrochemical biosensor for glucose detection. Mater. Sci. Eng. C **107**, 110273 (2020). https://doi.org/10.1016/j.msec.2019.110273
37. H.J. Cheon, M.D. Adhikari, M. Chung, Magnetic nanoparticles-embedded enzyme-inorganic hybrid nanoflowers with enhanced peroxidase-like activity and substrate channeling for glucose biosensing. Adv. Healthc. Mater. **8**, 1–8 (2019). https://doi.org/10.1002/adhm.201801507
38. N.L.D. Perera, J. Betancourt, J. Miksovska, K.E. O'Shea, Detail study on the interaction between perfluorooctanoic acid (PFOA) with human hemoglobin (Hb). Curr. Res. Toxicol. **5**, 100130 (2023). https://doi.org/10.1016/j.crtox.2023.100130
39. S. Tan, S. Yougbar, H. Chu, T. Kuo, Hemoglobin-conjugated gold nanoclusters for qualitative analysis of haptoglobin phenotypes. Polymers (Basel) **12**(10), 2242 (2020)
40. A. Kanwal, B. Saif, A. Muhammad, Hemoglobin-promoted growth of polyhedral gold nanoparticles for the detection of glucose, H_2O_2, and ascorbic acid. ACS Appl. Nano. Mater. **6**, 4734–4746 (2023). https://doi.org/10.1021/acsanm.3c00062
41. K. Wang, Y. Sun, W. Xu, Non-enzymatic electrochemical detection of H_2O_2 by assembly of CuO nanoparticles and black phosphorus nanosheets for early diagnosis of periodontitis. Sens. Actuators B Chem. **355**, 131298 (2022). https://doi.org/10.1016/j.snb.2021.131298
42. H. Jafari-nodoushan, S. Mojtabavi, M. Ali, Organic-inorganic hybrid nanoflowers : the known, the unknown, and the future. Adv. Colloid Interface Sci. **309**, 102780 (2022). https://doi.org/10.1016/j.cis.2022.102780
43. Z. Zhang, Y. Zhang, R. Song, Manganese(II) phosphate nanoflowers as electrochemical biosensors for the high-sensitivity detection of ractopamine. Sens. Actuators B Chem. **211**, 310–317 (2015). https://doi.org/10.1016/j.snb.2015.01.106
44. J. Li, M.C. Leu, R. Panat, J. Park, A hybrid three-dimensionally structured electrode for lithium-ion batteries via 3D printing. Mater. Des. **119**, 417–424 (2017). https://doi.org/10.1016/j.matdes.2017.01.088
45. V. Narwal, N. Yadav, M. Thakur, C.S. Pundir, An amperometric H2O2 biosensor based on hemoglobin nanoparticles immobilized on to a gold electrode. Biosci. Rep. **37**(4), BSR20170194 (2017). https://doi.org/10.1042/BSR20170194
46. W. Wu, Y. Fang, C. Zhu, Fabrication of highly stable and sensitive electrochemical sensor from hemoglobin-Au nanocomposites and its analytical applications. RSC Adv. **7**(68), 42884–42890 (2017). https://doi.org/10.1039/c7ra05808j
47. Z. Wu, Z. Wang, Y. Zhang, Amino acids-incorporated nanoflowers with an intrinsic peroxidase-like activity. Sci. Rep. **6**, 22412 (2016). https://doi.org/10.1038/srep22412
48. R. Mandavkar, S. Lin, M.A. Habib, Ultra-sensitive H_2O_2 sensing with 3-D porous Au/CuO/Pt hybrid framework. Sens. Actuators B Chem. **396**, 134512 (2023). https://doi.org/10.1016/j.snb.2023.134512
49. J. Anojčić, K. Kullawanichaiyanan, S. Mutić, Self-assembled iridium(III) complex microspheres on the carbon paste electrode surface for signal enhanced amperometric determination of H_2O_2 in color cream developers. J. Electroanal. Chem. **904**, 115873 (2022). https://doi.org/10.1016/j.jelechem.2021.115873
50. P. Murugan, R.D. Nagarajan, A.K. Sundramoorthy, Electrochemical detection of H_2O_2 using an activated glassy carbon electrode. ECS Sens. Plus **1**, 034401 (2022). https://doi.org/10.1149/2754-2726/ac7c78
51. J. Lu, Y. Hu, P. Wang, Electrochemical biosensor based on gold nanoflowers-encapsulated magnetic metal-organic framework nanozymes for drug evaluation with in-situ monitoring of H2O2 released from H9C2 cardiac cells. Sens. Actuators B Chem. **311**, 127909 (2020). https://doi.org/10.1016/j.snb.2020.127909
52. L. Zhang, Y. Wang, Y. Wang, Electrochemical H_2O_2 sensor based on a Au nanoflower-graphene composite for anticancer drug evaluation. Talanta **261**, 124600 (2023). https://doi.org/10.1016/j.talanta.2023.124600